Surface Engineering of 3D Gas Diffusion Electrodes for High Performance H_2 Production with Non-Precious Metal Catalysts

Joel Sanchez, [†‡] *Thomas R. Hellstern,* [†] *Laurie A. King,* *[†‡] *and Thomas F. Jaramillo* *[†‡§]

[†]Department of Chemical Engineering and [‡]SUNCAT Center for Interface Science and Catalysis, Stanford University, Stanford, California 94035, United States

[§]SLAC National Accelerator Laboratory, 2575 Sand Hill Road, Menlo Park. California 94025, United States

KEYWORDS: cobalt phosphide, electrode engineering, hydrogen evolution reaction, hydrophilicity

*Corresponding authors: Laurie A. King (lking10@stanford.edu) and Thomas F. Jaramillo (jaramillo@stanford.edu)

TOC Figure

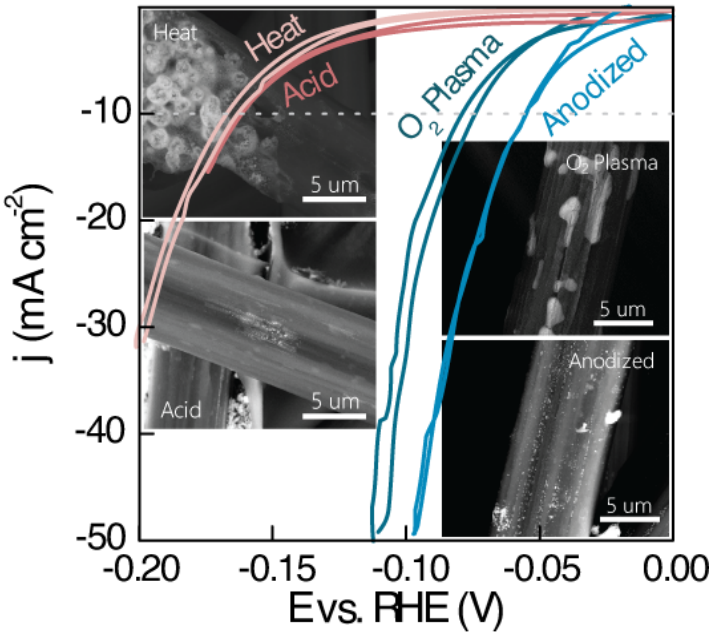

SHORT SUMMARY

Highly active transition metal phosphide hydrogen evolution catalysts with low overpotentials, unprecedented mass activities, high turnover frequencies, and promising durability are prepared by modifying the wetting properties of the underlying electrode. The origin of the improved performance is linked to an improved catalyst dispersion and morphology enabling high surface area CoP formulations at low-loadings.

ABSTRACT

In this work, we demonstrate a methodology to engineer gas diffusion electrodes for non-precious metal catalysts. We prepared highly active transition metal phosphides on carbon-based gas diffusion electrodes with low catalyst loadings by modifying the O/C ratio at the surface of the electrode. These non-precious metal catalysts yield extraordinary performance as measured by low overpotentials (-51 mV at -10 mA cm^{-2}), unprecedented mass activities (>800 A/g at 100 mV overpotential), high turnover frequencies (6.96 H_2 s^{-1} at 100 mV overpotential), and high durability for a precious metal free catalyst in acidic media. We find that a high O/C ratio induces a more hydrophilic surface directly impacting the morphology of the CoP catalyst. The improved hydrophilicity, stemming from introduced oxyl-groups on the carbon electrode, creates an electrode surface that yields a well-distributed growth of cobalt electrodeposits and thus a well-dispersed catalyst layer with high surface area upon phosphidation. This report demonstrates the high performance achievable by CoP at low loadings which facilitates further cost reduction, an important part of enabling the large-scale commercialization of non-PGM catalysts. The fabrication strategies described herein offer a pathway to lower catalyst loading while achieving high efficiency and promising stability on a 3D electrode.

INTRODUCTION

A diverse portfolio of clean energy technologies is paramount for the decarbonization of our society.[1] Water electrolyzers provide a route to decarbonization by making direct use of renewable energy to power H_2 production, mitigating the use of fossil fuels that are conventionally employed for H_2 production. Synergistically, they also enable the storage of excess energy during peak load hours in the form of chemical bonds in H_2. Hydrogen can then be directly consumed as

an energy carrier in internal combustion engines or in fuel cells, or, it can be implemented as a green feedstock in industrial processes such as the Haber-Bosch process, hydrocracking, and hydrodsulfirzation.[2] Water electrolysis is the combination of two half reactions, at the cathode – hydrogen evolution – and at the anode – oxygen evolution which enable the conversion of excess electrical energy to a chemical fuel. To date, platinum-based catalysts have been employed for the hydrogen evolution reaction (HER) in PEM-electrolyzers.[3] However, the high costs and price volatility associated with Pt motivate the investigation of non-platinum-group metals (PGM) based catalysts[3]. One possible solution is the lowering of Pt loading. Due to the high intrinsic activity of Pt towards the HER, high utilization efficiencies have been achieved with Pt at microgram (<50 $\mu g/cm^2$ in a device configuration and <10 $\mu g/cm^2$ in a three-electrode configuration) levels of loading.[4–7] Alternatively, tremendous efforts have been undertaken with the goal of developing non-noble metal catalysts that have the desirable performance activities of Pt without the high associated costs, scarcity, and price volatility.[8]

Recently, non-PGM based catalysts such as transition metal sulfides, phosphides, and carbides have been identified as promising electrocatalysts that have demonstrated low overpotentials for the HER while exhibiting excellent stability under acidic conditions.[9–12] Unfortunately, for non-PGM HER catalysts, a gap in intrinsic activity exists when compared to Pt and much work has been done to improve their activity[10]. In general, this is achieved by either increasing the number of active sites (e.g., through nanostructuring or increased loading) or increasing the intrinsic activity of the catalyst.[1] Although these approaches are effective to increasing overall reaction rates, there are physical limits as to how much catalyst can be loaded on an electrode without negatively affecting important processes, such as charge and mass transport.[13] This is further exacerbated in a 3D electrode configuration where catalyst distribution

is crucial for optimal catalyst performance.[14,15] 3D electrodes are viable electrocatalyst supports due to their high surface areas, electrical conductivity, and gas permeation for improved product separation and efficiencies. Studies on electrocatalysts supported on 3D electrodes have suggested that synthesizing the catalyst directly on the electrode can improve the stability and performance by enhancing catalyst-support interactions.[16–19] Furthermore, pretreating or modifying the support also has been demonstrated to improve performance.[20–22] Consequently, for various non-PGM electrode configurations, an increase in performance is often accomplished by increasing the catalyst loading. [16–19,23–27] While this strategy increases the number of catalyst surface sites, it may lead to low mass activities, low utilization efficiencies, and/or poor charge/mass transport, all of which lead to higher capital expenditures. Notwithstanding the advancements of non-PGM catalysts, concurrent studies have focused on decreasing the costs of PGM systems by minimizing the Pt loading through engineering and optimizing catalyst-support interactions. This motivates investigations into engineering catalyst support interactions to fabricate highly active electrodes at low loadings for non-PGM catalysts.

To probe the role of these possible synergistic factors and to achieve highly active non-PGM HER catalysts at low loadings, this work focuses on improving the hydrophilicity of the electrode in order to achieve a well-dispersed catalyst layer with high surface area that achieves high performance metrics at a low-loading. Utilizing various oxidation methods, the surface O/C ratio, and thus the hydrophilicity, is varied and is directly correlated to the cobalt phosphide dispersion onto the surface of the carbon electrode. Herein, we report a translatable methodology to achieve high performance catalysts at low-loadings for various phosphides where a high O/C ratio on the surface of the carbon electrode produces highly active catalysts that achieve low overpotentials, high mass activities, high turnover frequencies, and promising stability on a 3D

electrode configuration. Specifically, we focus our attention on a promising HER catalyst – CoP as a representative platform for this work. To the best of our knowledge, this is the first comparative study on various oxidation pretreatment methods for the well-dispersed growth of amorphous low-loading CoP on a 3D electrode carbon support.

RESULTS AND DISCUSSION

Electrochemical Performance of Low-loading CoP Cathodes

The general electrode fabrication process is shown in **Scheme 1**. All catalysts were synthesized directly onto high surface area carbon paper (Toray TGP-H-120, FuelCellStore – 1 cm^2) (**Figure S1**). In brief, transition metal-phosphide (Co, Fe, and Ni) catalysts were synthesized by first electrodepositing the metal oxide onto the carbon paper followed by a vapor phase phosphidation.[24] Prior to electrochemical deposition, however, the as-received carbon paper was treated by one of several different oxidation methods: O_2 plasma, anodization in a phosphate buffer

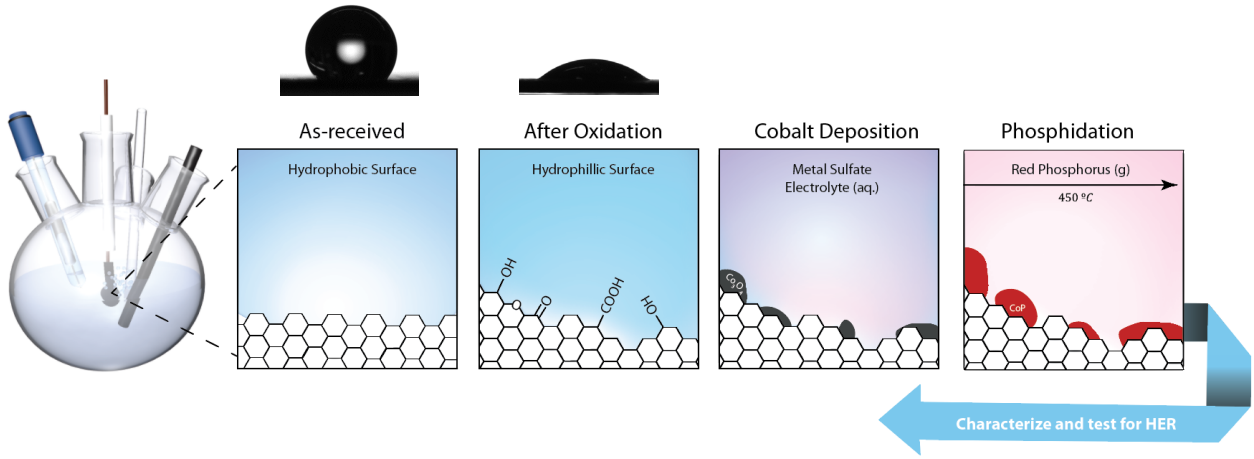

Scheme 1: Schematic illustration depicting the three-step synthesis of the transition metal phosphide cathodes in this work. The first panel represents the hydrophobic interface of our as-received Toray-120 followed by a surface oxidation treatment (O_2 plasma, anodization, acid treatment, or a heat treatment) of the electrode which introduces oxygen functional groups. Areas that have little to no oxygen groups remain hydrophobic and leave areas inaccessible to the metal electrolyte solution. Conversely, areas with a high O:C concentration are preferential sites for electrodeposition for metal oxide nanoparticles which are then phosphidized to form the transition metal phosphide.

solution, an acid treatment in a 12 M HNO_3 solution, or a heat treatment in air. Catalyst loading was controlled by the charge passed during electrochemical deposition (0.1, 0.5, 1.0, 1.5 and 2.0 C cm^{-2}) and quantified by ICP-MS.

As-prepared CoP electrodes were investigated by x-ray photoelectron spectroscopy (XPS) and x-ray diffraction (XRD). XPS (**Figure S2**) confirms the presence of the corresponding elements (Co^{2+} and P^{3-}) in high loading CoP catalyst and corroborate with previous CoP reports signifying the successful synthesis of CoP on our electrodes.[23,28] XRD patterns (**Figure S3**) for all CoP cathodes displayed broad peaks, or featureless diffractograms possibly due to the small crystallite size or the amorphous nature of the catalysts.

The HER activity of the synthesized CoP cathodes was assessed in a three-electrode cell under a constant purge of H_2 gas in 0.5 M H_2SO_4 electrolyte through cyclic voltammograms (CVs) (**Figure S4**). As shown in **Figure 1**, common metrics for benchmarking HER catalysts were assessed and are as follows: (1) the comparison of the overpotential required to achieve a current density of -10 mA cm^{-2} (η_{-10}); (2) the mass activities and (3) turnover frequencies at a specific overpotential defined here at -100 mV; and (4) as shown in **Figure 2**, the electrochemical stability through chronopotentiometry and accelerated cyclic voltammograms.[29] The overpotential measured at -10 mA cm^{-2} is the potential difference between the thermodynamic reduction potential of H_2 and the potential to achieve -10 mA cm^{-2}. Mass activity is a commonly used metric in the assessment of PGM-based catalysts corresponding to the absolute current normalized to the mass of the catalyst at a specific overpotential. Although it is uncommon in the HER literature, mass activity is also an important metric for non-PGM catalysts to probe the utilization efficiencies of catalysts, to assess the implications on mass transport, and to estimate for the relative cost of a system.[30,31] Turnover frequency (TOF) measurements describe the number of hydrogen

molecules evolved per second per surface site and is used as a metric for the intrinsic activity of the catalyst at the molecular level. Moreover, stability measurements asses the durability of the catalyst and are used as an important metric when considering the practicality of the electrode towards commercial applications. These performance metrics along with others can be found in Table 1.

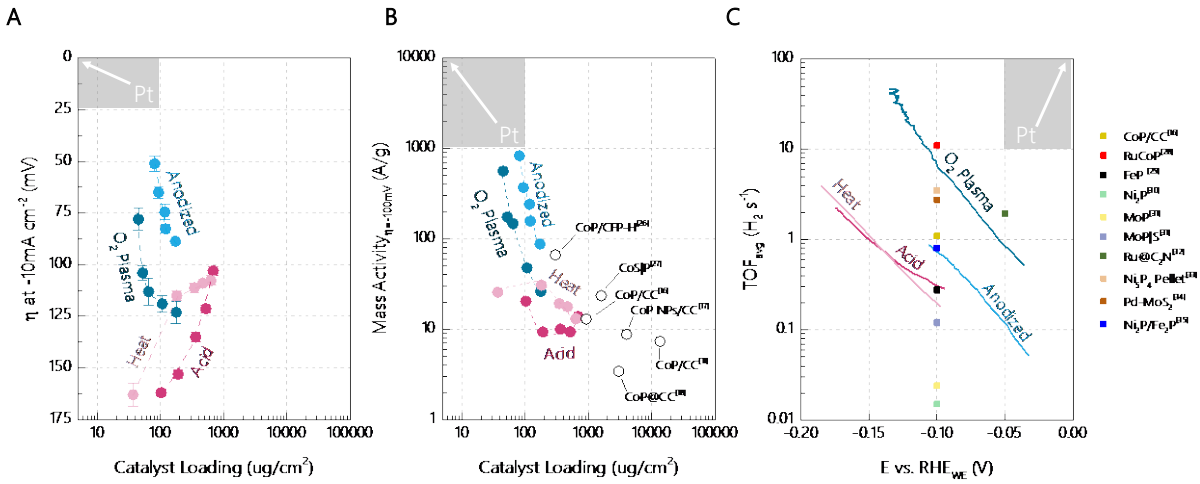

Figure 1: (A) Overpotential at -10 mA cm^{-2} versus catalyst loading plot of oxidized (anodized, O2 plasma, acidified, and heated) Toray-120 CoP cathodes. **(B)** Mass activities at 100 mV overpotential of all CoP cathodes in this work versus catalyst loading. For comparison, A and B include several representative CoP catalysts synthesized on a 3D electrode configuration. **(C)** Total electrode surface-site-averaged turnover frequency (TOF_{avg}) values of CoP-based cathodes at 0.1 C of charge passed (lowest loading) compared to other highly active HER catalysts in the literature.[17,38–45] Note, lines are drawn to guide the eye. For comparison, the range of performance of Pt is represented as gray shaded boxes in each panel.[5,54–56]

Regarding overpotential, **Figure 1A** illustrates the trends in η_{-10} as a function of CoP loading with reported state-of-the-art 3D CoP based catalysts.[16–19,32,33] For the samples presented in this work, the overall overpotential trends at -10 mA cm^{-2}_{geo} for low-loading systems are Anodized > O_2 plasma > Acid ≈ Heat and at high loadings Anodized > Acid > Heat > O_2 plasma. Interestingly, two opposing trends in overpotentials were observed for the synthesized electrodes as a function of catalyst loading. For the acid and heat-treated cathodes, a decrease in overpotential was observed at higher loadings. This is likely due to an increased CoP coverage and thus an increase in the number of active sites available for HER as correlated with an increase in

electrochemical surface area (ECSA) (**Table 1 and Figure S4B)**.[23] Strikingly, O_2 plasma treated and anodized CoP cathodes performed best at lower catalyst loadings. This is even more surprising given that the ECSA for these two systems increases as a function of increased catalyst loading implying that other factors give rise to the observed activity at low loadings.

Due to the large range in ECSA values (5 – 200 cm^2) presented in this work, normalizing to these values provides valuable insight for assessing the intrinsic activity of these catalysts.[34–36] The ECSA-normalized activity and the corresponding overpotential at any fixed current density will remain constant irrespective of catalyst loading if the morphology of the catalyst remains conformal (e.g. the deposition of 5 nm particles vs the growth and agglomeration of 5 nm particles into 10 nm particles at higher loadings). Such factors that evolve as a function of loading have been shown to impact the charge transfer of the catalyst-support.[34,37] To this end, low and high loading catalyst normalized were compared by their overpotentials required to achieve -0.2 mA cm^{-2}_{ECSA} . The overpotential trends for low-loading systems are O_2 plasma (34 mV) > Anodized (74 mV) > Heat (110 mV) > Acid (126 mV) and for high-loading systems are Heat (65 mV) > Acid (101 mV) > Anodized (122 mV) > O2 Plasma (146 mV). Comparing low-loading systems on a geometric and ECSA basis, the trends in overpotential are quite similar, where the anodized and O_2 plasma treated electrodes achieve lower overpotentials than their acid and heat treated counterparts. The switch in ranking between O2 plasma achieving a smaller overpotential than an anodized system is due to the lower ECSA of the low-loading O2 plasma electrode and possible contributions from the 20% lower charge transfer resistance relative to the anodized electrode (Table 1). For high-loading systems, this trend is reversed and through this ECSA normalization it is clear that the high geometric current density achieved by O_2 plasma and anodized systems stems predominantly from the high-surface area formulation. Although the trend that anodized and

O_2 plasma are more active at low loadings in relation to their high loading counterparts still holds on an ECSA basis and could potentially stem from lower charge transfer resistance and improved morphology as further discussed below.

Table 1: Comparison of loading, Tafel slopes, ECSA, R_{ct}, overpotential, mass activity, and TOF of all CoP cathodes presented in this work

Catalyst	Loading (mg cm^{-2})	Tafel Slope (mV dec^{-1})	ECSA (cm^2)	R_{ct} at η = 100 mV (ohms)	η @ -10 mA cm^{-2}_{geo} (mV)	η @ -0.2 mA cm^{-2}_{ECSA} (mV)	Current at η = 100 mV (mA cm^{-2})	Mass Activity at η = 100 mV (A/g)	TOF at η = 100 mV (H_2 s^{-1})
0.1 C Anodized	0.081	52	115.6	4.6	51	74	-67.00	827.55	0.93
2.0 C Anodized	0.172	78	191.9	7.6	88	122	-15.10	87.88	0.13
0.1 C O_2 Plasma	0.045	48	5.8	3.9	78	34	-24.97	559.87	6.96
2.0 C O_2 Plasma	0.177	84	103.4	5.0	123	146	-4.65	26.25	0.072
0.1 C Heat	0.037	58	7.6	94.1	163	110	-0.95	25.75	0.302
2.0 C Heat	0.630	80	11.5	36.6	106	65	-8.24	13.07	0.662
0.1 C Acid	0.103	70	11.1	165.2	162	126	-2.09	20.37	0.199
2.0 C Acid	0.683	75	22.9	14.1	102	101	-9.48	13.88	1.15

In terms of mass activity, **Figure 1B** shows the mass activities of the CoP electrodes compared to several reported high-performing (η_{-10} > -150 mV) 3D CoP electrodes in the literature.[16–19,32,33] By varying the oxidation method, the deposition charge and thus the catalyst loading, the prepared electrodes span a range of performance metrics and achieve mass activities two orders of magnitude higher when compared to the state-of-the-art electrodes **(Table S1)** signifying the high utilization efficiency achieved by our catalysts on a 3D electrode support.[17,38–45]

In our work, we considered the possibility that the support surface itself could contribute to catalytic activity. Studies have shown that the pretreatment of carbon electrodes introduces oxyl-groups and defects on the surface that result in active catalytic support systems towards the HER at values more negative than -600 mV vs RHE.[22] Similar results have been found with the phosphiditation of carbon supports leading to the formation of phosphorene which has also shown catalytic activity towards the HER.[46] To this end, we oxidized carbon electrodes and oxidized carbon electrodes that underwent phosphidation and investigated their HER activity. Figure S4A and S5B show that these pre and post treatments led to enhanced activity of the catalyst support

itself, though not sufficiently active to compete with the CoP catalysts within the operating potential range presented in this work (-200-0 mV vs RHE) indicating that the enhancement in activity does not directly stem from the support, though indirect contributions by means of catalyst-support interactions could still be possible.

For the TOF calculation (see supplemental information for full details), we assume that all surface sites, obtained through ECSA measurements, of Co and P atoms are catalytically active giving rise to TOF_{avg}. It should be noted that due to the nature of ECSA measurements, the TOF_{avg} values reported here include the capacitance contributions of the carbon electrodes. Accordingly, capacitance values of the bare oxidized carbon electrodes were obtained at the same potential window as our CoP loaded electrode and have found that the contribution from the carbon is minimal in comparison (**Figure S6)**; therefore, the values reported here allow for reasonable estimates of the TOF_{avg}. At low loadings, O_2 treated and anodized cathodes at η = -100 mV reach TOF values that are the highest in the literature among non-PGM catalysts on various electrode configurations (**Figure 1C and Table S1**). As an example, when compared to high performance CoP cathodes, our O_2 plasma treated cathode at the lowest loading (44.6 μg) at η = -100 mV achieved a TOF (6.96 H_2 s^{-1}) that is 14.5 times higher than that previously reported for a planar CoP[24] (0.48 H_2 s^{-1}) and 151 times higher than that of a high surface area CoP[23] (0.046 H_2 s^{-1}). To the best of our knowledge, on a TOF_{avg} basis, our system is the highest performing non-precious metal HER catalyst, surpassed only by a catalyst that employs Ru in a RuCoP configuration. The high utilization efficiency shown here for a CoP system showcases how catalyst-support interactions can be leveraged to improve non-PGM phosphide-based systems in order to reduce loading and improve performance.

To demonstrate the translatability of the methodology presented in this work, iron and nickel-based phosphide catalysts were also synthesized and characterized similarly to the cobalt phosphide system, using the anodization pretreatment only. An improvement in performance at lower loadings was observed for all the assessed systems (Figure S7) and provides evidence that the advantages demonstrated by this methodology is translatable to other non-PGM electrocatalytic systems. The overpotentials for the Fe and Ni systems have much room for improvement compared to CoP noting an opportunity for further optimization of the electrodeposition solution and the surface chemistry of the electrode. Mixed metal phosphides such as FeCoP are also promising catalytic systems worthy for their exploration using the methodologies presented herein.[9]

Electrocatalytic stability is a critically important factor in assessing the overall performance of an electrocatalyst. Reports where CoP is grown directly on the surface of a 3D support at high loadings have suggested that the catalyst-support interactions are improved to a point where little to no polymer binder is necessary.[16,17] At these high loadings, the degradation of CoP is negligible compared to the total loading of the cathode signifying that a large percentage of the catalyst remains for electrocatalysis.[16,17] Herein, we investigated the stability of our lowest loading electrodes with no polymeric binder by chronoamperometry, holding the electrodes at -10 mA cm^{-2} for >8 h. Interestingly, **Figure 2A** shows increased stability ($\Delta \approx 10$ mV) as a function of time

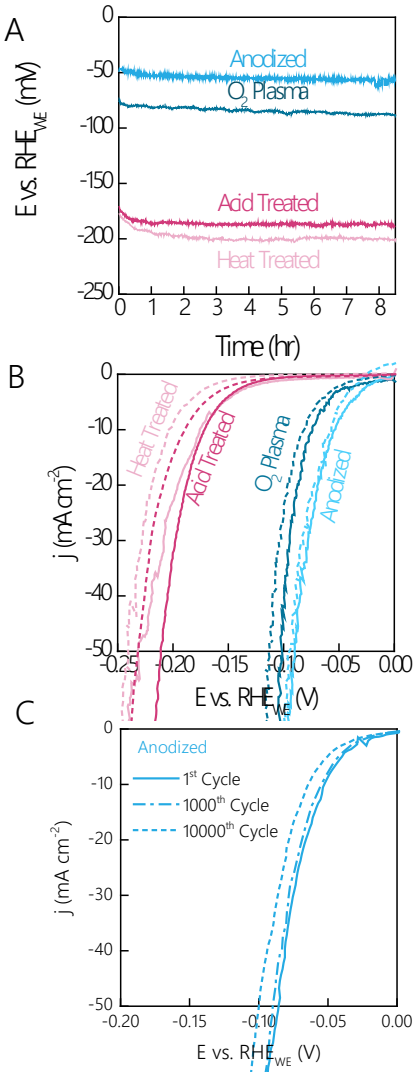

Figure 2: (A) Chronopotentiometric (CP) curves recorded at a constant current density of -10 mA cm^2 for all low loading (0.1 C of charge passed) CoP cathodes and **(B)** their respective cyclic voltammogram measurements before and after stability testing. **(C)** Accelerated durability testing for a CoP catalyst (low loading, anodized) at the 1st, 1000th, and 10000th cycle.

for the anodized and O_2 plasma treated electrodes in comparison to the heat and acid treated electrodes which lose activity more readily ($\Delta \approx$ 20-30 mV) over the >8 h stability measurements. We postulate that higher oxygen content (discussed below) on the surface for anodized and O_2 plasma treated cathodes improves the adhesion of cobalt oxide during electrodeposition thus resulting in better electrochemical stability when compared to their acid and heat-treated counterparts. Additionally, the more positive overpotentials exhibited by anodized and O_2 plasma treated electrodes for the same current densities may assist in perturbing further reduction reactions which may lead to phase, chemical, and structural changes of the electrode which can inhibit electrochemical stability.[47] Furthermore, accelerated durability testing was performed for the highest performance electrode (anodized, lowest loading) electrode and CVs for the 1st, 1000th, and 10000th cycle are shown in **Figure 2C**. After the 1000th cycle, a slight overpotential difference ($\Delta \approx$ 3 mV) is observed between the 1st (η_{-10} = 51 mV) and the 1,000th (η_{-10} = 54 mV) cycle. After the 10000th cycle a larger overpotential difference ($\Delta \approx$ 12 mV) between the 1st and the 10000th cycle (η_{-10} = -63 mV) is observed. Furthermore, the charge passed by CoP in this long-term stability testing is 2-3 orders of magnitude

higher (288 C cm^{-2}) when compared to the charge (0.087-0.262 C cm^{-2}) if CoP were to fully corrode. The small loss in geometric activity of the CoP electrodes (40-200 μg) with no polymeric binder after the extremely rigorous stability protocols underscores the promising durability of these low-loading systems towards applications in real-world devices.

To probe the difference in overpotential trends and to explain the high mass activities and turnover frequencies along with the stability measurements, further characterization was employed to investigate differences in the surface chemistry on the carbon electrodes after oxidation treatments and their effect on cobalt oxide dispersion during electrodeposition.

Surface Modifications of Toray-120

Contact angle measurements for the as-received and oxidized Toray-120 electrodes are shown in Figure 3. O_2 plasma ($\theta_c = 12.2^o$) treated and anodized ($\theta_c = 28.4^o$) electrodes resulted in contact angles in the hydrophilic regime ($\theta_c < 90^o$) whereas heat ($\theta_c = 114.9^o$) and acid ($\theta_c = 114.5^o$) treated electrodes showed a small decrease in contact angle from the as-received Toray-120 and remained hydrophobic in character ($\theta_c > 90^o$). To probe the surface chemistry post oxidation, XPS was used to obtain surface O/C ratios and high-resolution O and C 1s scans (**Table S2** and **Figure S8 and S9**). Compared to the as-received Toray-120 (O/C ratio ≈ 0.0), the heat and acid treated electrodes revealed a low (<0.1) O/C ratio compared to (>0.5) the O/C ratio of O_2 plasma treated and anodized electrodes. Furthermore, high resolution O 1s XPS shows that the surface of the carbon electrodes containing a mixture of carbon oxygen groups between 531 and 533 eV. All oxidized electrodes show a O1s spectral line in the 533 eV range which is indicative of –O functional groups in hydroxyls, ethers, lactones, and/or carboxyls. In addition, all oxidized electrodes besides anodized ones depicted spectral lines in the 532 eV range indicative of –O

functional groups in ethers, alcohols, and/or esters. For the anodized electrode an O 1s peak at 531 eV is representative of =O functional groups that can either be from carbonyls, lactones, anhydrides, and/or carboxyls while also having the possibility of arising from a P=O from a phosphate group. Various reports have shown that the oxidative pretreatment of carbon electrodes can introduce surface oxyl-groups and carbon defects that increase the performance of the supports with and without a catalyst.[21,22,25,48–50] Although similar surface chemistries are found in this work, these oxyl-groups have no direct impact on the electrochemical activity of the supports within the operating potential range of the tested CoP catalysts (Figure S3A). Instead, the role of these oxyl-groups is suggested to provide for an oxygen-rich surface where well-dispersed cobalt electrodeposits are possible as discussed below.

To probe the oxygen distribution of the oxidized electrodes, Auger electron spectroscopy (AES) elemental mapping was performed. As shown in **Figure 3B**, the oxidation process for heat and acid treated electrodes display small regions of an oxygen rich surface where the oxygen content is more prominent on the heat-treated electrodes. Areas that remain carbon rich and oxygen rich are believed to be hydrophobic and hydrophilic, respectively, thus possibly exhibiting a range of hydrophilicity within the surface area of the fibers at the microscale. Conversely, O_2 plasma treated and anodized electrodes showed a homogeneous coverage of oxygen content on the surface; therefore, qualitatively, the amount of oxygen content displayed in these maps is consistent with the trends observed in the O/C ratios obtained by XPS. Overall, the introduction of C-O and/or C=O containing surface groups increased the hydrophilicity of the carbon electrodes by creating a more oxygen rich surface with improved wetting properties.

To determine the role of these improved wetting properties on the CoP dispersion and morphology on the carbon electrodes, back scattered electron mode scanning microscopy (BSE

SEM) was utilized for the lowest and highest loading CoP cathodes (**Figure 4**). BSE SEM was used to readily distinguish CoP from that of the carbon support where areas with a higher atomic mass will appear at a higher brightness. As a function of charge passed, a wide range of morphologies and coverages were observed for each of the different oxidation pretreatments and loadings. At low CoP loadings, top-down micrographs (**Figure 4A and 4B)** for acid and heat

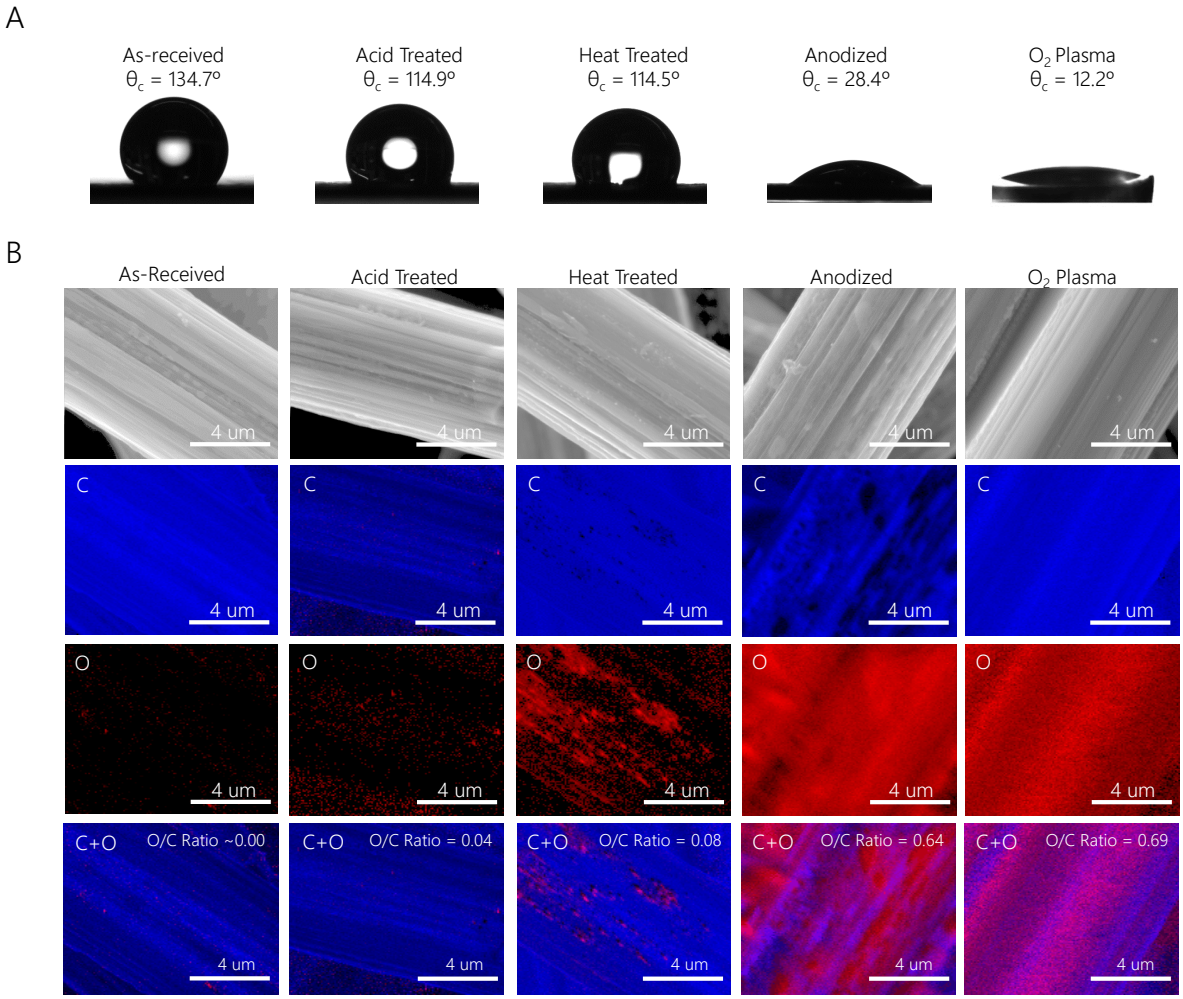

Figure 3. (A) Contact angle measurements for as-received and oxidized Toray-120 electrodes. (B) Top row displays SEM micrographs of as-received and oxidized Toray-120 electrodes and bottom row displays Scanning AES maps of combined carbon (blue) and oxygen (red) intensity on the surface of as-received and oxidized Toray-120 electrodes. O/C ratios are obtained from XPS measurements found in Table S2. Darker and brighter regions represent lower and higher atomic concentrations, respectively.

treated cathodes displayed non-uniform distributions of CoP on the electrode fibers whereas at higher loadings, CoP was uniformly distributed either on or in-between the fibers of the electrodes.

At these low loadings, CoP is not uniformly distributed across the surface of the electrode forming large agglomerates or layers that are found on or within the void of the fibrous network. At high loadings, the CoP dispersion drastically improves for the heat-treated samples where a slight to moderate improvement is observed for the acid treated samples. Conversely, at low loadings, the coverage of CoP is uniform and well dispersed for anodized and O_2 plasma treated electrodes

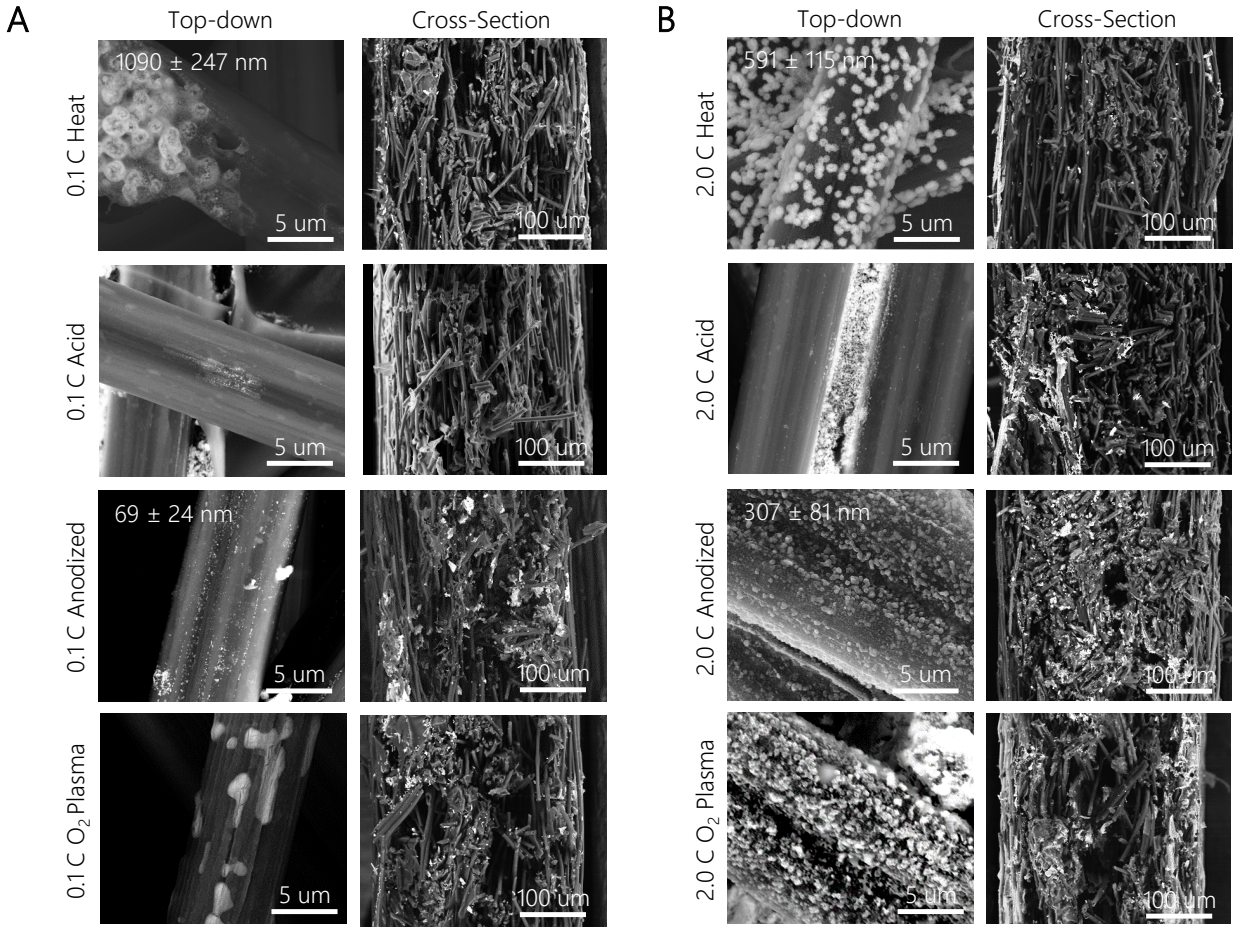

Figure 4. Top-down and cross-sectional backscattered-electron SEM micrographs of as-synthesized CoP electrodes at (**A**) low loadings (0.1 C of charge passed) and (**B**) high loadings (2.0 C of charge passed). The brighter regions represent the stronger electron scattering from higher Z number atoms (Co) in relation to the carbon support.

producing nanoparticles <100 nm and "thin-film" like morphologies on the carbon fibers, respectively. Similarly, at higher loading, the distribution of CoP was widely distributed on the surface and within the electrode. Although well dispersed, the CoP on the anodized sample exhibited larger nanoparticles (300-400 nm) that completely covered the carbon electrode surface

and most of the cross section of the electrode. For the O_2 plasma treated electrodes, the "thin-film" like morphologies of CoP were non-existent at higher loadings and appear to fully cover the surface of the nanofibers as dense films while having a more complete coverage of the cross section of the electrode. We ascribe these morphological differences to the low and high O/C content on the surfaces of the oxidized electrodes; therefore, we speculate that hydrophobicity/hydrophilicity of the carbon paper plays a major role in the nanostructuring of the electrode, which can greatly impact the electrode's catalytic performance. Additionally, the growth of CoP within the cross-section is visible through BSE SEM cross sections and AES mapping (Figure 4B and Figure S10). This growth within the cathode is likely due to the increased penetration depth of the electrolyte during electrodeposition. Furthermore, from the dispersion of the carbon-oxygen coverage as displayed in AES mapping (**Figure 3B**), it is evident that a higher O/C ratio (O_2 plasma treated and anodized) correlates to a more uniform CoP coverage and dispersion on the surface of the carbon fibers as well as throughout the 3D electrode itself.

Ultimately, the data suggests that a catalyst support with optimal wetting properties, such as a high O/C ratio, induces an optimal hydrophilic surface for cobalt nucleation during electrodeposition. This results in a uniform CoP distribution onto and within the 3D carbon electrode allowing for more accessible catalytic sites during reaction. With an improved understanding of the catalyst morphology we are now posed to further discuss the performance trends that were observed previously.

In terms of the dissimilar current-voltage trends, and correlating these to the SEM micrographs, we postulate that for low-loading samples, the dispersion of CoP is improved with higher O/C ratios. For the low O/C ratio samples, the distribution of CoP is improved at higher loadings as catalyst agglomeration is less of an issue. For the high O/C ratio samples, CoP remains

well-distributed through the electrode across a range of loadings and appears to grow thicker and deeper into the electrode at a higher loading. This has the potential to block the porous structure of the 3D electrode and therefore negatively affect performance. A thicker CoP layer, especially in a 3D electrode, would negatively affect mass and charge transport during catalysis. In essence, an ideal distribution of CoP was obtained at high O/C ratios and at low loadings.

We have identified two key experimental factors that may play a role in the high TOF and mass activities for our CoP cathodes on a 3D support: improved morphology and improved interfacial electron transfer between the carbon electrode and the catalyst. The improved wetting, as shown in Figure 3A, of the electrode achieved by our oxidation methodologies allows for favorable deposition between the electrode and the cobalt oxide electrolyte during electrodeposition. We postulate that hydrophobic regions are minimized due to a high O/C ratio, allowing for an increased number of carbon fiber sites that are accessible for electrodeposition. Similarly, since more sites are available for electrodeposition, that equates to a higher probability of attaining a well dispersed catalyst layer as evident by the SEM micrographs in Figure 4. We also posit that the direct electrodeposition of cobalt oxide, which is subsequently converted into CoP on a 3D electrode, creates an environment for improved electron transport between CoP and the underlying electrode which is crucial for electrocatalysis. To illustrate the improved electron transport, electrochemical impedance spectroscopy (EIS) was carried out at an overpotential of 100 mV for all low and high loading catalysts, as shown in the Nyquist plots in Figure S11. The charge transfer, R_{ct}, was compared for the low and high loading electrodes and is shown in Table 1. Note that many charge transfer resistances contribute to the measured R_{ct} value. Herein, we show that the R_{ct} values of our systems decrease with increased loading for heat and acid pretreated electrodes. The inverse is however true for the anodized and O2 plasma treated electrodes, where

R_{ct} values increase as a function of higher loading. While this is consistent with the trends observed in the TOF, this cannot alone account for the order of magnitude increase in TOF values observed by the low-loading O2 Plasma catalyst. For example, we postulate that factors such as the unique thin-film morphology of the 0.1 C O2 Plasma sample can provide for improved local charge polarization inducing local changes that are favorable for electrocatalysis such as improved local pH and improved mass transport.[50] Furthermore, catalyst-support interactions have been shown to perturb the electronic structure of the catalyst, leading to improved activity.[51] Such phenomena require further investigations for a deeper understanding of the origins of the high TOF. In summary, engineering the surface of a 3D electrode with distinct and optimized morphologies is an effective strategy to obtain active and stable catalysts at low-loadings.

CONCLUSION

Through surface modifications of 3D carbon paper electrodes, highly active CoP cathodes were synthesized that showed remarkable geometric activities at low loadings (~40-200 μg). Compared to reported electrodes, whether planar or 3D, in terms of mass activities and on a turnover frequency basis, our catalysts showed the highest values for non-PGM systems. The improved wetting properties of our electrodes improve the growth during electrodeposition, a key factor in achieving well-dispersed CoP catalysts in achieving catalysts with low charge transfer resistance that are highly active. Additionally, we show that the electrode fabrication process presented here is applicable to other phosphide catalysts and can be used as a general methodology to reduce catalyst loading, improve overpotentials, mass activities, and TOFs.

EXPERIMENTAL SECTION

Preparation of Carbon Paper Electrodes. All electrodes were prepared using TGP-H-120 (Toray, FuelCellStore), cut to a circular area of 1 cm^2 (Figure S1), and subsequently subjected to various surface oxidation methods described below. Acid treated electrodes consisted of the electrodes submerged in 10 mL of 12 M nitric acid (Fisher Chemical, Certified ACS Plus – 70%) at 70 ºC with gentle stirring (~60 RPM) and left to evaporate overnight. Heated electrodes were produced in a 3-temperature zone Mellen tube furnace (Mellen Company SC12.5R) in ambient atmosphere heated for 6 hours at 350 ºC (ramp rate of 1.5 ºC/min). Anodized electrodes were obtained by passing 2 C cm^{-2} at 1.65 V vs Ag/AgCl in a 50 mL 0.1 M phosphate buffer solution (Ricca Chemical Company, pH 7). Electrodes that underwent oxygen plasma treatment consisted of the electrodes in an oxygen plasma chamber *(Gala Instruments, PlasmaPrep5)* for 48 seconds at 100 W. All samples were thoroughly rinsed with deionized water after their respective oxidation procedure and left to dry overnight at room temperature before undergoing metal electrodeposition and further characterization.

Electrodeposition of Metal Oxide and Phosphidation of Carbon Paper Electrodes. To deposit cobalt oxide, the as-prepared oxidized electrodes were exposed to a reductive potential of -1.75 vs Ag/AgCl in a 100 mL 90 mM cobalt sulfate heptahydrate ($CoSO_4 \cdot 7H_2O$, Sigma-Aldrich, 98%), 90 mM boric acid (H_3BO_3, Sigma-Aldrich, 98%), and 12 mM sodium chloride (NaCl, Fisher Chemical, 98%) bath.[53] The total amount of charge passed during the cobalt electrodeposition was varied (0.1, 0.5, 1.0, 1.5, and 2.0 C) to obtain a variation of the cobalt loading. For Ni and Fe phosphides, the cobalt sulfate hydrate was replaced with a 100 mL 90 mM of nickel sulfate heptahydrate ($NiSO_4 \cdot 6H_2O$, Sigma-Aldrich, 99%) or a 100 mL 90 mM iron sulfate heptahydrate ($FeSO_4 \cdot 7H_2O$, Sigma-Aldrich, >99%), respectively. The metal oxide electrodes were then introduced into a 3-temperature zone Mellen tube furnace under a flow of 200 SCCM of H_2 gas

(Hydrogen Gas UHP, Airgas, 99.999%).[24] The phosphorous zone (closest to the inlet of H_2 gas – zone 1) contained of 0.5 g of red phosphorous (Red phosphorus, Sigma-Aldrich, ≥99.99%) and was heated to 450 ºC and the electrode zone (closest to the outlet of H_2 gas – zone 2 and 3) was heated to 375 ºC and both zones were held for 4 hours at a heating rate of 1.5 ºC/min. The electrodes were left to cool to room temperature within the furnace. After an hour of elapsed cooling time, the furnace was opened to allow for rapid cooling.

Hydrogen Evolution Reaction Activity. The HER activity of the cathodes was examined in a three-electrode configuration as presented in Scheme 1. A carbon rod counter electrode and a $Hg/HgSO_4$ (RREF0025, Pine) reference electrode were used for all measurements. The HER activity was determined by cycling the potential between 0.0 and -0.20 V versus the reversible hydrogen electrode (RHE) at 10 mVs^{-1} in H_2-saturated 0.5 M H_2SO_4 electrolyte. The solution resistance of the cell was measured by PEIS at 100 kHz and ohmic correction occurred after testing. The typical measured solution resistance was ~1-3 Ω. The reference electrode was calibrated using a Pt wire in 0.5 M H_2SO_4 after electrochemical testing.

Physical Characterization. The crystallinity of the catalysts was investigated using X-ray powder diffraction (Philips PANanalytical, Almelo, The Netherlands, X'Pert Pro) with Cu Kα radiation (λ = 1.54184 Å). The chemical state of Co, P, O, and C were examined using high-resolution x-ray photoelectron spectroscopy (PHI 5000 VersaProbe, Physical Electronics, Enzo, Chigasaki, Japan) with an Al Kα source and the C and O composition distribution was measured by Auger Electron Spectroscopy (PHI 700 Scanning Auger Nanoprobe, Physical Electronics, Enzo, Chigasaki, Japan) at 10kV and 10 nA electron gun beam voltage and current, respectively. All XPS spectra were calibrated to the adventitious carbon 1s peak at 284.8 eV and fitted using a Shirley background in CasaXPS. The atomic concentration of Co and P of the electrodes was

obtained through inductively coupled plasma mass-spectrometry (Thermo Scientific, XSERIES 2 ICP-MS) where the samples were digested in an aqua regia matrix before analysis. All calibration standards were TraceCERT® certified and obtained from Sigma-Aldrich. The top-down and cross-sectional micrographs were obtained with a FEI Magellan 400 XHR scanning electron microscope.

Author Contributions

The manuscript was written through contributions of all authors. All authors have given approval to the final version of the manuscript.

Funding Sources

Fundamental catalyst development was supported by the U.S. Department of Energy, Chemical Sciences, Geosciences, and Biosciences (CSGB) Division of the Office of Basic Energy Sciences, via Grant DE-AC02-76SF00515 to the SUNCAT Center for Interface Science and Catalysis. Electrode development and characterization was supported by the National Science Foundation (NSF) under the NSF Center for Chemical Innovation CHE-1305124 for Solar Fuels. The authors acknowledge that part of this work was performed at the Stanford Nano Shared Facilities (SNSF), supported by the National Science Foundation under award ECCS-1542152. J.S. acknowledges the Department of Defense (DoD) through the National Defense Science and Engineering Graduate Fellowship (NDSEG) Program and Stanford University Diversifying Academia, Recruiting Excellence Doctoral Fellowship Program (DARE).

References

[1] Z. Wei Seh, J. Kibsgaard, C. F. Dickens, I. Chorkendorff, J. K. Nørskov, T. F. Jaramillo, *Science* **2017**, *355*, eaad4998.

[2] R. Ramachandran, R. K. Menon, *Int. J. Hydrogen Energy* **1998**, *23*, 593.

[3] P. C. K. Vesborg, T. F. Jaramillo, *RSC Adv.* **2012**, *2*, 7933.

[4] Z. Kang, G. Yang, J. Mo, Y. Li, S. Yu, D. A. Cullen, S. T. Retterer, T. J. Toops, G. Bender, B. S. Pivovar, J. B. Green, F.-Y. Zhang, *Nano Energy* **2018**, *47*, 434.

[5] N. Cheng, S. Stambula, D. Wang, M. N. Banis, J. Liu, A. Riese, B. Xiao, R. Li, T.-K. Sham, L.-M. Liu, G. A. Botton, X. Sun, *Nat. Commun.* **2016**, *7*, 13638.

[6] X. Shang, Z.-Z. Liu, S.-S. Lu, B. Dong, J.-Q. Chi, J.-F. Qin, X. Liu, Y.-M. Chai, C.-G. Liu, *ACS Appl. Mater. Interfaces* **2018**, *10*, 43561.

[7] J. X. Wang, Y. Zhang, C. B. Capuano, K. E. Ayers, *Sci. Rep.* **2015**, *5*, 12220.

[8] X. Zou, Y. Zhang, *Chem. Soc. Rev.* **2015**, *44*, 5148.

[9] J. F. Callejas, C. G. Read, C. W. Roske, N. S. Lewis, R. E. Schaak, *Chem. Mater.* **2016**, *28*, 6017.

[10] P. C. K. Vesborg, B. Seger, I. Chorkendorff, *J. Phys. Chem. Lett.* **2015**, *6*, 951.

[11] Y. Shi, B. Zhang, *Chem. Soc. Rev. Chem. Soc. Rev* **2016**, *45*, 1529.

[12] J. D. Benck, T. R. Hellstern, J. Kibsgaard, P. Chakthranont, T. F. Jaramillo, *ACS Catal.* **2014**, *4*, 3957.

[13] J. Mo, Z. Kang, S. T. Retterer, D. A. Cullen, T. J. Toops, J. B. Green, M. M. Mench, F.-Y. Zhang, *Sci. Adv.* **2016**, *2*, e1600690.

[14] B. Bladergroen, H. Su, S. Pasupathi, V. Linkov, in *Electrolysis*, InTech, **2012**, pp. 45–60.

[15] H.-R. "Molly" Jhong, F. R. Brushett, P. J. A. Kenis, *Adv. Energy Mater.* **2013**, *3*, 589.

[16] X. Yang, A.-Y. Lu, Y. Zhu, M. N. Hedhili, S. Min, K.-W. Huang, Y. Han, L.-J. Li, *Nano Energy* **2015**, *15*, 634.

[17] J. Tian, Q. Liu, A. M. Asiri, X. Sun, *J. Am. Chem. Soc.* **2014**, *136*, 7587.

[18] Q. Li, Z. Xing, A. M. Asiri, P. Jiang, X. Sun, *Int. J. Hydrogen Energy* **2014**, *39*, 16806.

[19] Y. Cheng, F. Liao, W. Shen, L. Liu, B. Jiang, Y. Li, M. Shao, *Nanoscale* **2017**, *9*, 18977.

[20] J. Kibsgaard, T. F. Jaramillo, F. Besenbacher, *Nat. Chem.* **2014**, *6*, 248.

[21] X. Wang, W. Li, D. Xiong, D. Y. Petrovykh, L. Liu, *Adv. Funct. Mater.* **2016**, *26*, 4067.

[22] X. Niu, L. Shi, X. Li, J. Pan, R. Gu, H. Zhao, F. Qiu, Y. Yan, M. Lan, *Electrochim. Acta* **2017**, *235*, 64.

[23] E. J. Popczun, C. G. Read, C. W. Roske, N. S. Lewis, R. E. Schaak, *Angew. Chemie Int. Ed.* **2014**, *53*, 5427.

[24] T. R. Hellstern, J. D. Benck, J. Kibsgaard, C. Hahn, T. F. Jaramillo, *Adv. Energy Mater.* **2016**, *6*, 1501758.

[25] Y. Wang, B. Kong, D. Zhao, H. Wang, C. Selomulya, *Nano Today* **2017**, *15*, 26.

[26] J. Masa, S. Barwe, C. Andronescu, I. Sinev, A. Ruff, K. Jayaramulu, K. Elumeeva, B. Konkena, B. Roldan Cuenya, W. Schuhmann, *ACS Energy Lett.* **2016**, *1*, 1192.

[27] A. Ursua, L. M. Gandia, P. Sanchis, *Proc. IEEE* **2012**, *100*, 410.

[28] J. A. Cecilia, A. Infantes-Molina, E. Rodríguez-Castellón, A. Jiménez-López, *Appl. Catal. B Environ.* **2009**, *92*, 100.

[29] C. C. L. McCrory, S. Jung, I. M. Ferrer, S. M. Chatman, J. C. Peters, T. F. Jaramillo, *J. Am. Chem. Soc.* **2015**, *137*, 4347.

[30] C. G. Morales-Guio, L. Liardet, X. Hu, *J. Am. Chem. Soc.* **2016**, *138*, 8946.

[31] S. Zou, M. S. Burke, M. G. Kast, J. Fan, N. Danilovic, S. W. Boettcher, *Chem. Mater.* **2015**, *27*, 8011.

[32] S. H. Yu, D. H. C. Chua, *ACS Appl. Mater. Interfaces* **2018**, *10*, 14777.

[33] W. Liu, E. Hu, H. Jiang, Y. Xiang, Z. Weng, M. Li, Q. Fan, X. Yu, E. I. Altman, H. Wang, *Nat. Commun.* **2016**, *7*, 10771.

[34] S. Anantharaj, S. Kundu, *ACS Energy Lett.* **2019**, DOI 10.1021/acsenergylett.9b00686.

[35] D. Voiry, M. Chhowalla, Y. Gogotsi, N. A. Kotov, Y. Li, R. M. Penner, R. E. Schaak, P. S. Weiss, *ACS Nano* **2018**, DOI 10.1021/acsnano.8b07700.

[36] J. Kibsgaard, I. Chorkendorff, *Nat. Energy* **2019**, *4*, 430.

[37] Y. Zhang, Z. Xie, J. Wang, *ACS Appl. Mater. Interfaces* **2009**, DOI 10.1021/am900529e.

[38] J. Xu, T. Liu, J. Li, B. Li, Y. Liu, B. Zhang, D. Xiong, I. Amorim, W. Li, L. Liu, *Energy Environ. Sci.* **2018**, *11*, 1819.

[39] J. F. Callejas, J. M. McEnaney, C. G. Read, J. C. Crompton, A. J. Biacchi, E. J. Popczun, T. R. Gordon, N. S. Lewis, R. E. Schaak, *ACS Nano* **2014**, *8*, 11101.

[40] E. J. Popczun, J. R. McKone, C. G. Read, A. J. Biacchi, A. M. Wiltrout, N. S. Lewis, R. E. Schaak, *J. Am. Chem. Soc.* **2013**, *135*, 9267.

[41] J. Kibsgaard, T. F. Jaramillo, *Angew. Chemie Int. Ed.* **2014**, *53*, 14433.

[42] J. Mahmood, F. Li, S.-M. Jung, M. S. Okyay, I. Ahmad, S.-J. Kim, N. Park, H. Y. Jeong, J.-B. Baek, *Nat. Nanotechnol.* **2017**, *12*, 441.

[43] A. B. Laursen, K. R. Patraju, M. J. Whitaker, M. Retuerto, T. Sarkar, N. Yao, K. V. Ramanujachary, M. Greenblatt, G. C. Dismukes, *Energy Environ. Sci.* **2015**, *8*, 1027.

[44] Z. Luo, Y. Ouyang, H. Zhang, M. Xiao, J. Ge, Z. Jiang, J. Wang, D. Tang, X. Cao, C. Liu, W. Xing, *Nat. Commun.* **2018**, *9*, 2120.

[45] Y. Ge, P. Dong, S. R. Craig, P. M. Ajayan, M. Ye, J. Shen, *Adv. Energy Mater.* **2018**, *8*, 1800484.

[46] L. Shao, H. Sun, L. Miao, X. Chen, M. Han, J. Sun, S. Liu, L. Li, F. Cheng, J. Chen, *J. Mater. Chem. A* **2018**, DOI 10.1039/c7ta10884b.

[47] J. D. Benck, B. A. Pinaud, Y. Gorlin, T. F. Jaramillo, *PLoS One* **2014**, *9*, e107942.

[48] R. Bose, S. K. Balasingam, S. Shin, Z. Jin, D. H. Kwon, Y. Jun, Y.-S. Min, *Langmuir* **2015**, *31*, 5220.

[49] P.-C. Huang, S. Brahma, P.-Y. Liu, J.-L. Huang, S.-C. Wang, S.-C. Weng, M. Shaikh, P.-C. Huang, S. Brahma, P.-Y. Liu, J.-L. Huang, S.-C. Wang, S.-C. Weng, M. O. Shaikh, *Catalysts* **2018**, *8*, 462.

[50] M. Li, M. Yu, X. Li, *Appl. Surf. Sci.* **2018**, *439*, 343.

[51] N. Godino, X. Borrise, F. X. Muñoz, F. J. Del Campo, R. G. Compton, *J. Phys. Chem. C* **2009**, DOI 10.1021/jp9031354.

[52] C. T. Campbell, *Nat. Chem.* **2012**, DOI 10.1038/nchem.1412.

[53] T. M. Whitney, P. C. Searson, J. S. Jiang, C. L. Chien, *Science* **1993**, *261*, 1316.

[54] Z. Pu, I. S. Amiinu, Z. Kou, W. Li, S. Mu, *Angew. Chemie Int. Ed.* **2017**, *56*, 11559.

[55] R. Chen, C. Yang, W. Cai, H.-Y. Wang, J. Miao, L. Zhang, S. Chen, B. Liu, *ACS Energy Lett.* **2017**, *2*, 1070.

[56] I. J. Hsu, Y. C. Kimmel, X. Jiang, B. G. Willis, J. G. Chen, *Chem. Commun.* **2012**, *48*, 1063.